Computed Rate Coefficients and Product Yields for *c*-C₅H₅ + CH₃ → Products

Sandeep Sharma and William H. Green*

Department of Chemical Engineering, Massachusetts Institute of Technology, Cambridge, Massachusetts 02139

Received: January 22, 2009; Revised Manuscript Received: June 1, 2009

Using quantum chemical methods, we have explored the region of the C_6H_8 potential energy surface that is relevant in predicting the rate coefficients of various wells and major product channels following the reaction between cyclopentadienyl radical and methyl radical, c-C_5H_5 + CH_3. Variational transition state theory is used to calculate the high-pressure-limit rate coefficient for all of the barrierless reactions. RRKM theory and the master equation are used to calculate the pressure dependent rate coefficients for 12 reactions. The calculated results are compared with the limited experimental data available in the literature and the agreement between the two is quite good. All of the rate coefficients calculated in this work are tabulated and can be used in building detailed chemical kinetic models.

1. Introduction

The reaction between cyclopentadienyl radical and methyl radical, c-C_5H_5 + CH_3, is an important pathway toward benzene formation in combustion and pyrolysis.[1] Although the potential energy surface was computed in the 1990s by Melius et al.[2] and Moskaleva et al.,[3] more precise calculations are now possible. Even with an accurate PES, the calculation of the pressure dependent gas-phase rate coefficients is a challenging task. As can be seen in the potential energy surface in Figure 1, several loose transition states and chemically activated product channels are important at high temperatures.

Recently there have been considerable advances in the methodology for rate coefficient calculations for loose transition states.[4−7] In addition to these advances, there has been significant progress in accurate calculation of the pressure dependent rate coefficients for complicated potential energy surfaces with multiple wells and multiple product channels.[8−13] The method is based on the master equation formulation of the problem. These detailed equations are then appropriately coarse-grained to calculate the phenomenological rate coefficients.

In this paper we use both these methods to calculate the pressure dependent rate coefficients for the title reaction over a range of temperatures and pressures. These pressure dependent rate coefficients, the high pressure limit rate coefficients, and the thermochemistry of all of the reactions and species are provided for use in a detailed chemical kinetic models.

2. Theoretical Methodology

Figure 1 shows the potential energy diagram for the formation of fulvene and various C_6H_8 and C_6H_7 species by the title reaction. In addition to the product channels labeled in the figure, we have also calculated the energy of other high energy product channels and tabulated their energy relative to c-C_5H_5 + CH_3 in Table 1. For this study we have included only the 5 product channels shown in Figure 1. R5 channel has not been included even though it is a lower energy channel than R4 because there is a higher barrier toward the formation of R5, and when we performed calculations by including this product channel, its rate coefficient was lower than the R4 product channel by about 1 order of magnitude. The nomenclature used in Figure 1 and Table 1 is explained by Figure 2.

2.1. Quantum Chemistry. *2.1.1. Single-Reference Methods.* All single reference quantum chemical calculations described in this section are performed by the Gaussian 03 quantum chemistry package.[14] The potential energy diagram in Figure 1 was generated by performing calculations at the CBS-QB3 level of theory.[15−17] The method makes use of the fact that geometry is not very sensitive to the level of theory employed and so the geometry and frequencies are calculated at B3LYP/CBSB7 level of theory. This geometry is then used to perform higher level quantum calculations at CCSD(T)/6-31 g+(d') and MP4SDQ/CBSB4. The energies at these levels are used with the final step which incorporates some empirical correction factors to estimate energies of the CCSD(T) method with an infinite basis set. This method is widely used and should give energies accurate to within 2 kcal/mol.[17]

Ab initio calculations for all of the stable molecules, radicals, and tight transition states were also performed using the G2 method,[18] another method which should provide energies with an accuracy in the range of 2 kcal/mol.[19] The G2 method is based on a similar idea as the CBS-QB3 method, where the optimized geometry is calculated at the MP2/6-31G(d) level of theory and frequencies are calculated at the HF/6-31G(d) level of theory. Subsequently higher level methods including MP2/6-311+G(3df,2p), QCISD(T)/6-311G(d,p), and MP4/6-311+G(d,p) are used to calculate correlation energies. Finally an empirical correction is added to correct for correlation ignored by the QCISD(T) method and also to extrapolate to the infinite basis set limit. These two methods differ substantially in the type of extrapolation scheme they employ and give a set of values which can be compared to each other to check anomalously high differences in energies. For the transition states the negative frequency was visualized to validate the correctness of transition state.

2.1.2. Multireference Methods. In the potential energy surface shown in Figure 1 there are 7 transition states without an energy barrier. To compute the rate coefficients for these reactions, we use microcanonical variational transition state theory, which requires an accurate energy prediction of the potential energy along the bond breaking coordinate. Conventional single reference ab-intio methods fail to accurately predict the potential during bond breaking after the bond length increases beyond a certain length. For this reason we use the
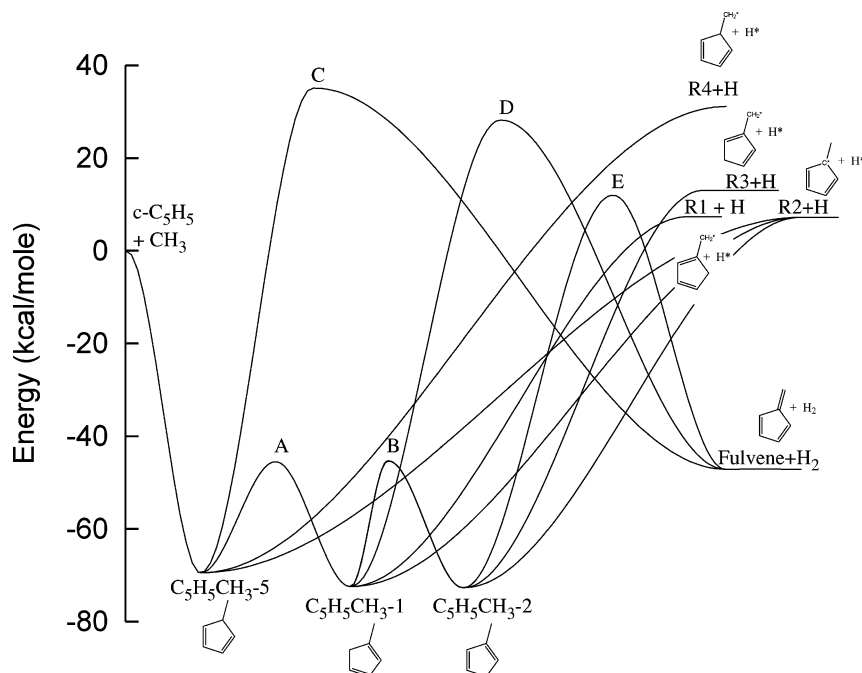
Figure 1. Potential energy diagram at CBS-QB3 level of theory for reaction of c-C_5H_5 with CH_3 calculated at 0 K.

TABLE 1: Various Possible Product Channels and Their Energies Relative to the Entrance Channel c-C_5H_5 + CH_3 Arranged in Ascending Order[a]

molecule	energy (kcal/mol)
fulvene + H_2	−47.13
R2 + H	7.20
R1 + H	7.34
R3 + H	13.00
R5 + H_2	20.73
R4 + H	31.10
C_5H_5-3 + CH_3	33.07
C_5H_5-2 + CH_3	33.59
R11 + H	40.77
R9 + H	41.14
R8 + H	41.55
R12 + H	41.71
R10 + H	41.81
R7 + H	44.07
R6 + H	44.76

[a] All of the energies are calculated using CBS-QB3 method and are at 0 K.

CASPT2 method[20,21] which is a multireference counterpart of the MP2 method, as implemented in MOLPRO.[22] The key problem in these methods is the selection of an appropriate active space. In general the active space should include all of the orbitals taking part in the bond breaking plus the π and π^* orbitals in the ring. First MCSCF calculations are performed with a given basis set and active space. The orbitals of the MCSCF calculations are used to then perform the CASPT2 calculations. The active space to include in CASPT2 calculations can be judged by looking at the occupation number of the orbitals.

We first calculate the potential for C−C bond fission in methylcyclopentadiene to form methyl and cyclopentadienyl radials. Table 2 shows the occupation numbers of different orbitals in the active space, when the active space consists of 8 orbitals and 8 electrons. The criteria we have used in our work is if an orbital has an occupation number greater than 1.97 or less than 0.03 then we do not include it in the active space. The table shows that at all bond lengths the 19th and 26th

orbitals do not need to be included in the active space based on our criteria. Figure 3 confirms that including electrons and orbitals beyond the required 6 does not add to the accuracy of the method. The potential energy calculated using 6e6o active space and 8e8o active space is the same, but the shape of the potential changes significantly if we make the active space smaller to 4e4o as is shown in Figure 3.

On the other hand the same figure shows that the inclusion of a larger basis set cc-pvtz as opposed to cc-pvdz makes the potential slightly (~1 kcal/mol) more attractive. This same effect was seen in some of the earlier papers by Klippenstein and Harding.[5,6] The cc-pvdz surface closely matches the cc-pvtz surface suggesting the basis set expansion has sufficiently converged by cc-pvtz.

2.2. Statistical Mechanics and Rate Calculations. For most of the molecules and the tight transition states, we have used a rigid rotor harmonic oscillator approximation with corrections added for internal rotors. The frequencies calculated using B3LYP/CBSB7 theory were scaled by a factor of 0.99 as recommended by Scott et al.[23] In molecules where there is a single bond between sp^3 and sp^2 carbon atoms we assumed that the rotation about that bond was barrierless so it was treated as a free rotor (e.g., the out of ring carbon carbon single bond in $C_5H_5CH_3$−1 has a rotational barrier of only 1.4 kcal/mol). The barriers for other internal hindered rotors were calculated by a relaxed scan at B3LYP/CBSB7 level. The scanned potential was fit to a Fourier series in the torsional angle ϕ; $V(\phi) = (A_m \cos(m\phi) + B_m \sin(m\phi))$ where m went from 0 to 5. The reduced moment of inertia based on the equilibrium geometry was calculated using the formulas described by Pitzer.[24−26] In this paper we have used the reduced moment of inertia $I^{(2,3)}$,[27] and the one-dimensional Schroedinger equation was solved numerically. For cyclopentadienyl an additional moment of inertia for pseudo rotation was used as described in section 3.1. For the calculations of heats of formation of stable molecules, bond additivity corrections (BAC) as recommended by Petersson[28] were also included. This BAC correction was not included in the calculation of the rate coefficients because reliable BAC values are not available for transition states, and including BAC
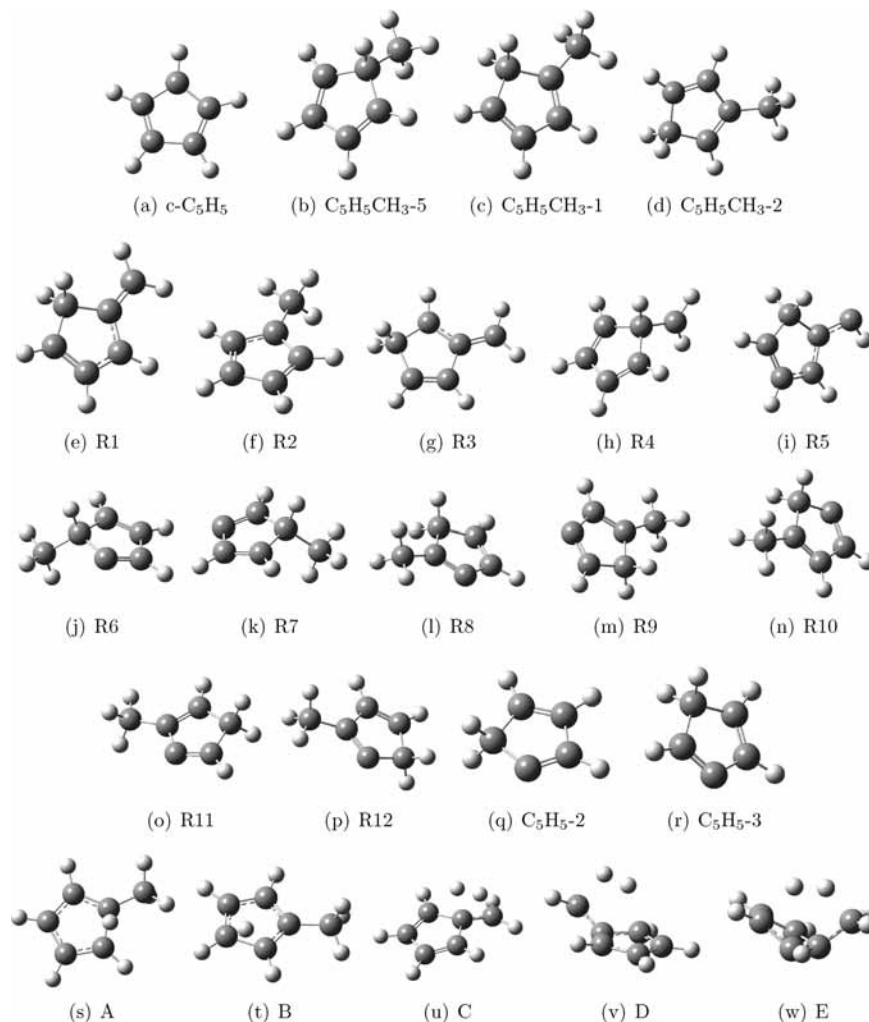
c-C$_5$H$_5$ + CH$_3$ → Products

J. Phys. Chem. A, Vol. 113, No. 31, 2009 **8873**

Figure 2. Names and structures of molecules and transition states. The negative frequency was visualized to validate the correctness of the transition state.

TABLE 2: Occupation Number of Different Orbitals in the Active Space for Various C−C Bond Distances, Using the cc-pvdz Basis

orbital	C−C bond length (A)								
	2.3	2.5	2.7	2.9	3.2	3.6	4.0	5.0	6.0
19	1.990	1.990	1.990	1.990	1.990	1.991	1.991	1.991	1.991
20	1.947	1.944	1.941	1.939	1.938	1.937	1.937	1.937	1.937
21	1.906	1.904	1.903	1.902	1.901	1.901	1.901	1.901	1.901
22	1.791	1.689	1.573	1.459	1.315	1.183	1.105	1.052	1.026
23	0.220	0.323	0.439	0.554	0.698	0.829	0.907	0.959	0.985
24	0.070	0.072	0.073	0.074	0.074	0.075	0.076	0.076	0.076
25	0.065	0.068	0.070	0.072	0.074	0.074	0.075	0.075	0.075
26	0.010	0.010	0.010	0.010	0.010	0.009	0.009	0.009	0.009

only in reactants can cause systematic errors in barrier heights. For tight transition states, canonical transition state theory was used, and tunneling was included by simple Wigner correction.[29]

2.2.1. Density of State Calculations in Variflex. In the calculations involving loose transition states and pressure dependent calculations, Variflex was used to calculate density of states and subsequently the rate coefficients. The details of the calculations have been described in Miller et al.[9] For all stable molecules and tight transition states, the rigid rotor harmonic oscillator approximation was used. The classical density of states corresponding to the hindered torsional motions was calculated as a phase space integral. An estimate of the quantum density of states was obtained using the Pitzer−Gwinn[24] approximation shown in eq 1, where $\rho_q^t(E)$ and $\rho_{cl}^t(E)$

are quantum mechanical and classical density of states for torsion and $\rho_q^{ho}(E)$ and $\rho_{cl}^{ho}(E)$ are the quantum mechanical and classical density of states obtained by treating the torsion as a harmonic oscillator.

$$\rho_q^t(E) = \rho_{cl}^t(E) \frac{\rho_q^{ho}(E)}{\rho_{cl}^{ho}(E)} \tag{1}$$

The difference between this estimate and the density of states for hindered rotors computed by solving the 1-d Schroedinger equation is not large for our system. The total sum of states $N(E)$ was calculated by convoluting this hindered rotor density
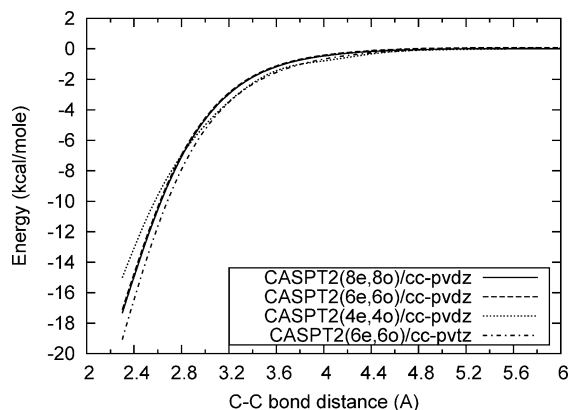
Figure 3. Comparison of potential curves using the CASPT2 method with different active spaces and basis sets. Increasing the active space beyond 6e,6o does not change the result significantly. The basis set of cc-pvtz makes the potential more attractive compared to cc-pvdz.

of state with the density of states of the other vibrational modes. The rotational states were calculated by assuming that in molecules at least two of the three principal moments of inertia were equal; that is, asymmetric tops were approximated as symmetric tops. For any given value of rotational quantum number J, the total number of states including vibrational and rotational states is calculated to obtain $N(E,J)$ by a method described by Miller et al.[30]

2.3. Variational Transition State Rate Calculation. We have used Variflex to calculate the rate coefficients for the loose transition states. A brief description of the method is presented below. The E, J resolved microscopic rate coefficient due to RRKM[31,32] theory is given in eq 2.

$$k(E,J) = \frac{N(E,J)}{h\rho(E,J)} \quad (2)$$

where the numerator is the sum of states of the transition state to energy E with angular momentum J and the denominator is the density of states of the reactants at the specified energy and angular momentum. In variational transition state theory, a dividing hypersurface which separates the reactants from the products is picked which minimizes the numerator in eq 2.

Here we use the assumption[33−35] whereby the internal modes of the transition states are divided into 1 reaction coordinate, 5 transitional modes (for two nonlinear fragments) which involve relative rotations of the fragments, and the remaining "conserved modes" which are vibrations of the separated fragments and are assumed to not change substantially along the reaction coordinate. The density of states of the conserved modes are calculated by applying the traditional rigid rotor harmonic oscillator approximation in which the frequencies of the separated fragments are used. The transitional modes are usually low frequency modes and the number of states of these modes with angular momentum $J\hbar$ and energy less than or equal to E at the dividing surface $s = s_0$ can be calculated using the semiclassical phase space integral shown in eq 3.[36]

$$N_{tr}(E,J,s_0) = \frac{\hbar}{h^n} \int \delta(s - s_0)\delta(E - H(\tau, p_s, s))\delta(J\hbar -$$

$$J_T(\tau, p_s, s))\Theta(\dot{s})\dot{s}\, d\tau\, ds\, dp_s \quad (3)$$

In this equation, s is the reaction coordinate and p_s is its conjugate momentum; τ has n coordinates, conjugate momenta

pair which include the transitional coordinates, conjugate momenta pairs, and an additional three pairs corresponding to external rotation of the whole molecule (for 2 nonlinear fragments $n = 8$), $H(\tau)$ is the classical Hamiltonian of the transitional modes, J_T is the magnitude of the classical angular momentum, and $\Theta(\dot{s})$ is the step function of $\dot{s}$ which is 0 for $\dot{s} < 0$ and 1 otherwise.

The reaction coordinate (s) can be picked in many ways, the easiest two being distance between the reacting atoms and the distance between the center of masses of the two fragments. For a rigorous calculations not only the transition state along the reaction coordinate is varied but also the definition of the reaction coordinate itself is varied to minimize the TST reaction rate. In our study we have decided to simplify the analysis by picking the definition of the reaction coordinate as the distance between the two bonding atoms. It has been previously pointed out[4] that the change of pivot point location within the reacting fragments can cause the computed rate of the reaction to decrease by 5%.

The integral in eq 3 contains 3 delta functions which are separately integrated out before using a Monte Carlo method for calculating the integral. The method has been described in detail by Klippenstein.[36] The sum of states of transitional modes is convoluted with the density of states of the conserved modes to get the total sum of states of a transition state.

The Hamiltonian $H(\tau)$ is the sum of kinetic energy and the potential energy. The potential energy is written as a sum of changes in potential (eq 4) 1. due to the change in the separation between the two fragments at a given interfragment orientation and 2. due to change in the interfragment orientation at a given separation.

$$V(s,\tau) \approx V_1(s, \tau_{fixed}) + V_2(s,\tau) - V_2(s, \tau_{fixed}) \quad (4)$$

Usually calculation of the first part of this potential (V_1) requires a high level of accuracy because interfragment separation represents bond-breaking or bond-forming, while the second part of this potential (V_2) is relatively easy to predict so a lower level method can be used. This same principle was used by Petersson[37] for development of the IRC-MAX calculations and by Klippenstein and Harding in their papers.[4,5]

To test this assumption we have calculated the high pressure rate coefficient for the entrance channel c-C_5H_5 + CH_3 using the CASPT2(6e,6o)/cc-pvdz and CASPT2(6e,6o)/cc-pvdz+CASPT2(2e,2o)/cc-pvdz methods. CASPT2(6e,6o)/cc-pvdz represents the method in which the potential used in the Monte Carlo method is calculated at the CASPT2(6e,6o)/cc-pvdz level of theory, but on the other hand, CASPT2(6e,6o)/cc-pvdz+CASPT2(2e,2o)/cc-pvdz represents a method in which V_1 is calculated using CASPT2(6e,6o)/cc-pvdz level of theory and the orientation dependence of the potential V_2 is calculated using CASPT2(2e,2o)/cc-pvdz. The results are plotted as shown in Figure 4. The maximum difference between the rate coefficients computed using the two methods is 35%. For our work here, we deem this as an acceptable level of accuracy given the fact that we get about a 1 order of magnitude savings in computation time.

Rate coefficients for all of the loose transition states presented in this paper were calculated using CASPT2(6e,60)/cc-pvtz+CASPT2(2e,2o)/cc-pvdz. For each transition state we have picked 9 interatomic separations ranging from 2.3 to 6.0 Å. For each separation we carried out 1000 CASPT2(2e,2o)/cc-pvdz calculations to calculate the sum of states of the transitional modes using the Monte Carlo method.
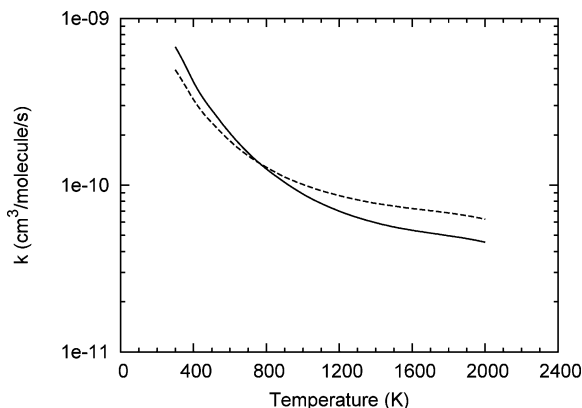
c-C$_5$H$_5$ + CH$_3$ → Products

J. Phys. Chem. A, Vol. 113, No. 31, 2009 **8875**

Figure 4. High pressure limit rate coefficients for reaction *c*-C$_5$H$_5$ + CH$_3$ → C$_5$H$_5$CH$_3$-5 predicted by the CASPT2(6e,60)/cc-pvdz+-CASPT2(2e,2o)/cc-pvdz (solid line) and CASPT2(6e,6o)/cc-pvdz methods (dashed line).

Our separation of conserved and the transitional modes neglects the change in geometry of the reacting fragments as they move closer to each other. It has been pointed out in an earlier paper by Harding et al.[4] that this approximation can cause the transition state position to decrease to very low interatomic separation at high *E*'s and *J*'s. In our work we have noticed the same trend and have restricted the loose transition state position to have interfragment distance >2.3 Å.

The *J*-averaged microcanonical rate coefficient *k*(*E*) was computed by

$$k(E) = \frac{1}{h}\frac{\Sigma_J N^{\ddagger}(E,J)(2J+1)\Delta J}{\Sigma_J \rho(E,J)(2J+1)\Delta J} \quad (5)$$

where Δ*J* is the discretization used for *J* and $N^{\ddagger}(E,J)$ and $\rho(E,J)$ are the sum of states of transition state and density of states of the reactant respectively; the canonical rate constant *k*(*T*) was computed by

$$k(T) = \frac{1}{h}\frac{\Sigma_E \Sigma_J N^{\ddagger}(E,J)(2J+1)e^{-E/k_BT}\Delta J\Delta E}{\Sigma_E \Sigma_J \rho(E,J)(2J+1)e^{-E/k_BT}\Delta J\Delta E} \quad (6)$$

where Δ*E* is the discretization used for *E*. In this work we have used Δ*E* = 75 cm^{-1} and Δ*J* = 25.

2.4. Master Equation and Phenomenological Rate Constant. We have calculated the pressure dependent rate coefficients for all the reactions in the PES shown in Figure 1 using Variflex. To calculate these pressure dependent rate coefficients Variflex solves the 1-D master chemical equation and uses the energy resolved microcanonical rate coefficients (*k*(*E*)) as calculated in Equation 5. For all the calculations the energy transfer probability for each collision assumes the exponential down model, with the energy transfer parameters for each bath gas used in this study provided in Table 3. The details of the formulation of the master equation and methodology of solution used in Variflex is described in detail elsewhere.[11−13,38,39]

3. Results and Discussion

3.1. Thermochemistry. We have performed CBS-QB3 and G2 calculations on each of the molecules in Figure 1. Figure 5 shows the difference between the atomization energy of different molecules and transition states calculated using the G2 and CBS-

TABLE 3: Energy Transfer Parameters Used in the Exponential Down Model for Bath Gas Ar (See Section 3.4), Kr,[40] and N$_2$[11a]

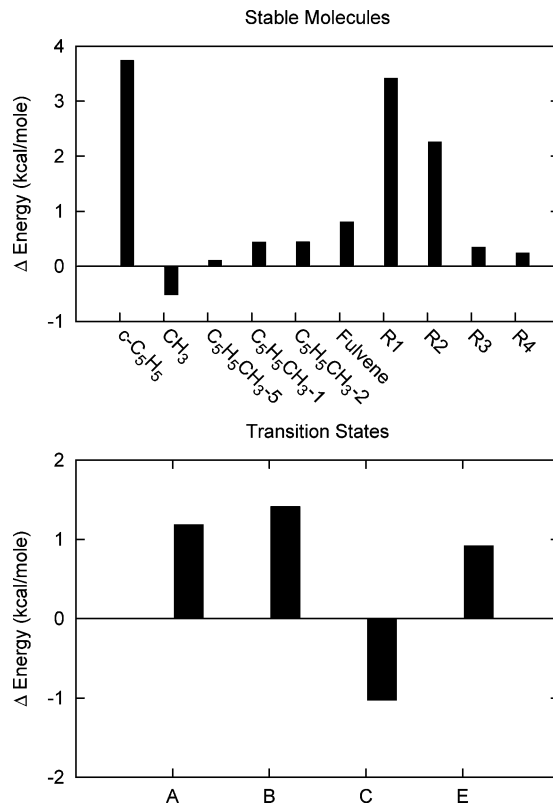| bath gas	⟨ΔE_d⟩
Ar	100
Kr	350
N$_2$	125

[a] All values have units of cm^{-1}.

Figure 5. Difference between the atomization energy using the G2 and CBS-QB3 methods. In the bottom part of the figure, all of the transition states are as labeled in the PES. We could not obtain a saddle point for transition state D using the G2 method, and hence, the comparison is not given here.

QB3 methods. The atomization energies predicted by G2 are systematically higher than the CBS-QB3 values. It has been noted earlier that the G2 method is deficient when it comes to predicting the heat of formation for unsaturated cyclic molecules.[41] To test this hypothesis we have performed calculations at the G3[41] level for the molecules which showed considerable discrepancy between the G2 and CBS-QB3 predictions. These molecules include *c*-C$_5$H$_5$, R1, and R2. The differences between the atomization energies between G3 and CBS-QB3 values for these three molecules are −0.29, −1.01, and +0.50 kcal/mol, respectively, whereas the difference between G2 and G3 is much higher. These small differences in G3 and CBS-QB3 atomization energies suggest that CBS-QB3 values are more accurate than G2 values for the present system, and we therefore used the energies calculated by the CBS-QB3 method. The predicted thermochemical properties for all of the molecules included in this study are presented in Table 4. Also the thermochemical values calculated by Melius et al.[2] using the BAC-MP4 method are compared to the ones calculated here using the CBS-QB3 method in Table 5.

***c*-C$_5$H$_5$.** There have been several studies of the Jahn−Teller effect on the energy levels of *c*-C$_5$H$_5$, which should allow

TABLE 4: Thermochemical Values Calculated Using the CBS-QB3 Level of Theory[a]

molecule	H_{298} kcal/mol	S_{298} cal/(mol K)	C_p (cal/(mol K))						
			300	400	500	600	800	1000	1500
c-C_5H_5	63.7	64.0	18.1	23.9	28.6	32.3	37.6	41.3	46.9
CH_3	35.2	47.9	9.5	10.2	10.9	11.6	12.9	14.1	16.3
$C_5H_5CH_3$-5	27.1	74.1	24.1	32.1	38.8	44.3	52.3	58.0	66.7
$C_5H_5CH_3$-2	23.9	75.8	23.3	31.0	37.7	43.2	51.5	57.5	66.4
$C_5H_5CH_3$-1	24.2	75.9	23.3	30.9	37.6	43.1	51.5	57.4	66.4
fulvene	52.7	70.2	21.7	28.8	34.6	39.3	46.1	50.8	57.9
R1	53.3	74.4	23.5	31.2	37.5	42.5	49.9	55.1	62.9
R2	53.3	77.1	23.4	30.6	36.7	41.6	48.9	54.1	61.9
R3	59.2	74.4	23.8	31.4	37.7	42.7	50.0	55.2	62.9
R4	77.2	77.8	23.4	30.8	36.9	41.8	49.0	54.1	61.8

[a] Special methods are used for cyclopentadienyl, see section 3.1.

accurate computation of its thermochemistry.[42–44] These studies recommend the usual rigid rotor harmonic oscillator approach for the treatment of the non Jahn–Teller active vibrational modes and a more rigorous treatment of Jahn–Teller vibrational modes. The treatment of the Jahn–Teller active modes is complicated by the coupling of the vibrational and electronic states due to the near degenerate electronic state of the molecule. In the rest of the section we give a brief description of this coupling and how its effect can be taken into account to calculate the vibronic states. For a more detailed derivation the reader can refer to one of the many good treatments available.[42,45,46] Our purpose here is to give enough detail so that the reader can appreciate what approximation we have used in writing our code which calculates the Jahn–Teller vibronic states.

We expand the vibronic states of the molecule as a summation given in Equation 7 where $|\Lambda(q_e)\rangle$ are the eigenstates of the electronic Hamiltonian defined in eq 9. In D_{5h} symmetry of cyclopentadienyl the ground state is 2-fold degenerate and the next excited state is energetically removed from them. Then due to Born–Oppenheimer approximations the summation over all electronic states is truncated to just the ones over the two degenerate ground states shown in Equation 8. In subsequent equations in this section we use the notation that q_e and p_e are the coordinates and conjugate momentum of the electrons and Q_n and P_n are the normal coordinates of the nuclei and their conjugate momenta. The origin of the nuclear coordinates is chosen so that all the normal coordinates Q_i in the vector Q_n are 0 at the lowest energy D_{5h} geometry and at this geometry Q_n is represented by Q_n^0.

$$|\Psi\rangle = \sum_{n,\Lambda} |\Lambda(q_e)\rangle |\xi^\Lambda(Q_n)\rangle \quad (7)$$

$$|\Psi\rangle = |\Lambda^1(q_e)\rangle |\xi^1(Q_n)\rangle + |\Lambda^{-1}(q_e)\rangle |\xi^{-1}(Q_n)\rangle \quad (8)$$

$$H_{el}(q_e, Q_n^0)|\Lambda(q_e)\rangle = \left(\sum_e \frac{P_e^2}{2} + V(q_e, Q_n^0)\right)|\Lambda(q_e)\rangle = E_{el}|\Lambda(q_e)\rangle \quad (9)$$

The next step is to expand the nuclear component of the wave function $|\xi(Q_n)\rangle$ as a linear combination of products of harmonic oscillator basis functions centered on the lowest-energy D5h geometry as shown in eq 10. In eq 10 $|\nu_{ji}\rangle$ is ket describing the wave function of the ith non Jahn–Teller vibrational mode with quantum number ν_{ji} and $|\nu_{jdi}, l_{jdi}\rangle$ describes the wave function of

the ith degenerate Jahn–Teller mode in the state with quantum numbers ν_{jdi} and l_{jdi}.

$$|\xi^1(Q_n)\rangle = \sum_{\nu_{j1},...,\nu_{jdp}, l_{jdp}} A^1_{j1,...,jd1,...,jdp}|\nu_{j1}\rangle|\nu_{j2}\rangle...|\nu_{j3N-6-2p}\rangle \times$$
$$|\nu_{jd1}, l_{jd1}\rangle|\nu_{jd2}, l_{jd2}\rangle...|\nu_{jdp}, l_{jdp}\rangle \quad (10)$$

The full electronic plus nuclear Hamiltonian is written and simplified to a form given in eq 11. In this equation the first and second derivatives have been calculated at the lowest energy D_{5h} geometry.

$$\begin{aligned}
H(q, Q) &= \left(\sum_n \frac{P_n^2}{2} + \sum_e \frac{P_e^2}{2m_e} + V(q_e, Q_n)\right) \\
&= \left(\sum_n \frac{P_n^2}{2} + H_{el}(Q_n^0) + \Delta V(q_e, Q_n)\right) \\
&= \left(\sum_n \frac{P_n^2}{2} + H_{el}(Q_n^0) + \sum_i \frac{\partial V}{\partial Q_i}Q_i + \sum_i \frac{\partial^2 V}{\partial Q_i^2}Q_i^2\right)
\end{aligned} \quad (11)$$

We can write the Hamiltonian operator as a matrix using the basis set defined in eq 8. The resulting Hamiltonian matrix is diagonalized to calculate the vibronic energy levels. For a full derivation of the matrix elements for a Jahn–Teller molecule we refer the reader to comprehensive review written by Barckholtz and Miller.[42]

In eq 11 the nonzero value of $\langle\Lambda^\pm(q_e)|(\partial V)/(\partial Q_i)|\Lambda^\mp(q_e)\rangle$, where Q_i represents a normal mode corresponding to a Jahn–Teller active mode, gives rise to off-diagonal matrix elements in the Hamiltonian matrix. These nonzero off-diagonal matrix elements cause the linear perturbation in V along the Jahn–Teller vibrational modes.

The non Jahn–Teller modes do not couple directly with the Jahn–Teller modes. Thus these modes can be treated as the usual harmonic oscillators to calculate the partition functions. For a given Jahn–Teller mode only those off-diagonal elements are nonzero that couple modes having the same Jahn–Teller quantum number j defined by $j = l - \Lambda/2$, where Λ is the electronic quantum number and takes on values 1 or −1. The fact that there is coupling between modes with the same j is used to convert the Hamiltonian into a block diagonal form where each block corresponds to a specific value of j and is solved independently.

$$|\pm\rangle|\nu_1,l_1\rangle|\nu_2+1,l_2\pm 1\rangle$$

$$\updownarrow$$

$$|\pm\rangle|\nu_1-1,l_1\pm 1\rangle|\nu_2,l_2\rangle \quad \leftrightarrow \quad |\mp\rangle|\nu_1,l_1\rangle|\nu_2,l_2\rangle \quad \leftrightarrow \quad |\pm\rangle|\nu_1+1,l_1\pm 1\rangle|\nu_2,l_2\rangle$$

$$\updownarrow$$

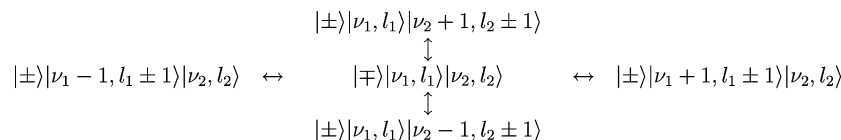$$|\pm\rangle|\nu_1,l_1\rangle|\nu_2-1,l_2\pm 1\rangle$$

Figure 6. Given vibronic state $|\mp\rangle|\nu_1,l_1\rangle|\nu_2,l_2\rangle$ having Jahn−Teller quantum numbers $j_1 = l_1 \pm 0.5$ and $j_2 = l_2 \pm 0.5$ can couple directly with 5 other states having the same values of j_1 and j_2.

TABLE 5: Comparison of Heats of Formation of Reactants, Wells, and Product Channels Calculated Using the CBS-QB3 and BAC-MP4 Methods

	H_{298} (kcal/mol)	
molecule	CBS-QB3	BAC-MP4[a]
c-C$_5$H$_5$ + CH$_3$	98.9	98.8
C$_5$H$_5$CH$_3$-5	27.1	25.8
C$_5$H$_5$CH$_3$-2	23.9	23.7
C$_5$H$_5$CH$_3$-1	24.2	23.7
R1 + H	105.4	104.8
R2 + H	105.4	106.5
R4 + H	129.3	132.1

[a] From ref 2. The difference between the values calculated by CBS-QB3 method and BAC-MP4 method in the worst case of R4 + H is less than 3 kcal/mol and in other cases is about 1 kcal/mol.

Different Jahn−Teller modes couple with each other via a second order coupling in which say a mode $|\Lambda^+\rangle|\nu_{i1},l_{i1}\rangle|\nu_{i2},l_{i2}\rangle$ is coupled to $|\Lambda^-\rangle|\nu_{i1}+1,l_{i1}-1\rangle|\nu_{i2},l_{i2}\rangle$ and also to $|\Lambda^-\rangle|\nu_{i1},l_{i1}\rangle|\nu_{i2}+1,l_{i2}-1\rangle$ giving rise to coupling between the latter two modes. Figure 6 shows a schematic of how a given vibronic state containing two Jahn−Teller active modes are coupled to five other vibronic states. Having this coupling greatly increases the size and number of the blocks of the Hamiltonian, where each block now represents a pair of Jahn−Teller quantum numbers j_1 and j_2. Similarly having three active Jahn−Teller modes further increases the size of the Hamiltonian blocks to be diagonalized. We have written a small python code which can calculate the energy levels and subsequently entropy of the Jahn−Teller active modes with up to two modes coupled with each other. This code is later used to calculate the entropy of cyclopentadienyl (code available in the Supporting Information).

To calculate the Hamiltonian matrix and then the energy levels, we first need the vibrational frequencies ω_i and their contribution to the linear Jahn−Teller stabilization energy D_i for the E'_2 Jahn−Teller vibrational modes. Kiefer et al.[43] have calculated the frequencies using finite differences of the analytical first derivative of CASSCF/cc-PVDZ method at the conical intersection and found a negative mode of frequency −6345 cm^{-1} as the only active mode which gives rise to a 1655 cm^{-1} stabilization energy. Applegate et al.[47,48] have performed detailed ab initio calculations along with spectroscopic experiments to calculate the stabilization energy and active Jahn−Teller vibrational modes. They have used GRHF[49] to calculate the vibrational frequencies of the unperturbed molecule and then partitioned the Jahn−Teller stabilization energy between 3 of the 4 E'_2 modes as shown in Table 6. Using these parameters they have got a good agreement with experimentally observed spectrum. Due to the unusual nature of the potential energy at the conical intersection it is difficult to judge whether either of the two methods used gives the correct values of the Jahn−Teller frequencies.

In yet another approach, Katzer and Sax[44] have developed a general procedure for computing the moment of inertia for pseudorotations in Jahn−Teller active molecule. According to this procedure the vibrational frequencies of the perturbed molecule are calculated and treated as harmonic oscillators and

TABLE 6: Jahn−Teller Active Mode Vibrational Frequencies and Values of D_i[47a]

mode	ω_i (cm^{-1})	D_i
I	815	0.22
II	1058	0.36
III	1411	0.68

[a] D_i is the contribution of each mode to Jahn-Teller stabilization. For example 815 cm^{-1} mode with $D_i = 0.22$ causes $815 \times 0.22 = 179$ cm^{-1} Jahn-Teller stabilization.

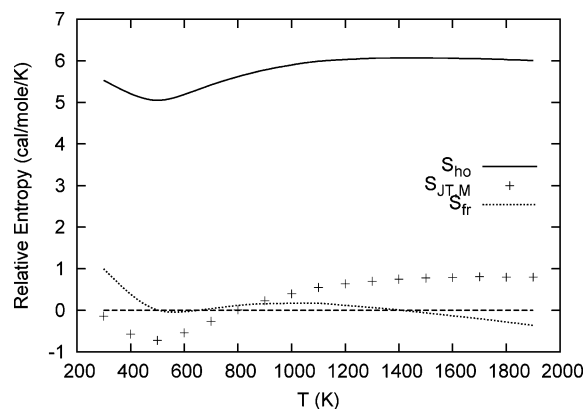**Figure 7.** c-C$_5$H$_5$ entropy calculated using three different methods relative to the values recommended by Kiefer et al.[43] which is represented by the dashed line at 0 cal/mol/K. For S_{ho} all modes of vibrations of a distorted molecule were treated as harmonic oscillators, for S_{fr} the ultra low frequency of a distorted molecule is treated as a free rotor, and $S_{JT,M}$ is the entropy calculated by diagonalizing the Hamiltonian using parameters suggested by Applegate et al.[47] (see text).

the low frequency vibration corresponding to pseudorotation of the molecule is treated as a free rotor. At B3LYP/CBSB7 level of theory the $^2B_1$ and $^2A_2$ structures with C_{2v} symmetry are a first order saddle point and a third order saddle point respectively. Instead we have performed B3LYP/CBSB7 calculation for cyclopentadienyl without using symmetry. The final optimized structure shows one ultra low frequency mode of 25 cm^{-1} which corresponds to the pseudorotation. The rotational constant to be used when calculating the partition function of the free rotor for pseudorotation is taken from the work of Katzer and Sax as 230 cm^{-1}. The rest of the modes are treated as harmonic oscillators.

In this paper we are mainly concerned about the thermochemistry of the cyclopentadienyl molecule and we use the different methods to calculate the entropy of cyclopentadienyl radical as a function of temperature. The results, plotted in Figure 7, suggest that the difference between the various approaches for the Jahn−Teller effect is not very large and is within the accuracy of the methods involved. For the calculation of partition function and entropy $S_{JT,M}$ (see Figure 7), we have treated the three Jahn−Teller modes independently of each other. These three modes are actually coupled to each other. The coupling effect is important when one is looking at spectroscopic data, but it turns out to be not important when one is interested in calculating macroscopic properties like entropy. We have
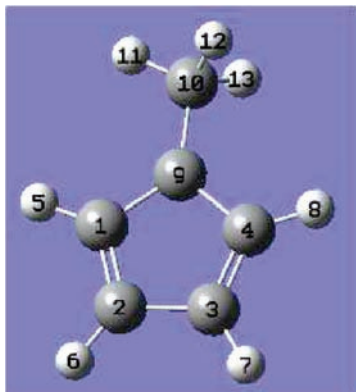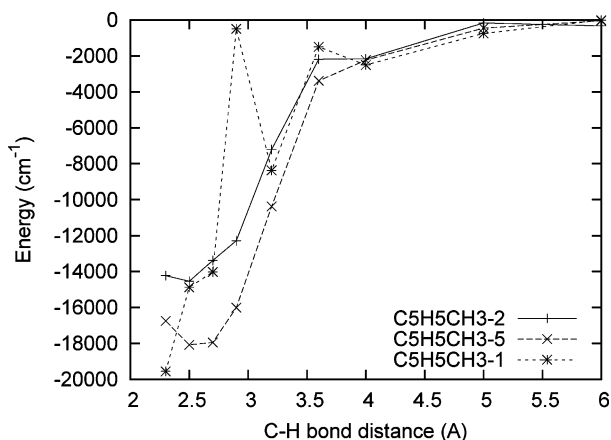
Figure 8. Optimized geometry of R2.

Figure 9. Minimum potential energy path for reaction of R2 with H to form $C_5H_5CH_3$-5, $C_5H_5CH_3$-1, and $C_5H_5CH_3$-2. The anomalous point for $C_5H_5CH_3$-1 is spurious (see the text).

Figure 10. High-pressure-limit rate coefficients of barrierless reactions. The list of legends is +, c-C_5H_5+CH_3 → $C_5H_5CH_3$-5; ×, R2 + H → $C_5H_5CH_3$-5; *, R2 + H → $C_5H_5CH_3$-1; □, R1 + H → $C_5H_5CH_3$-1; ■, R2 + H → $C_5H_5CH_3$-2; ○, R3 + H → $C_5H_5CH_3$-2; ●, R4 + H → $C_5H_5CH_3$-5.

compared the entropy contribution of the two Jahn−Teller modes with frequencies 815 and 1058 cm^{-1}, with and without the coupling between the modes, and found them to be equal to two decimal places. The purely rigid rotor harmonic oscillator approach using the B3LYP/CBSB7 frequencies results show a significant amount of error when compared to the other methods. In the rest of the paper, we have used the Katzer and Sax approach to treat cyclopentadienyl because of its good accuracy and relative computational simplicity.

3.2. High Pressure Rate Constant Calculations. Figure 8 shows the optimized geometry of R2. A hydrogen atom can add to carbon 9 to form $C_5H_5CH_3$-5, to carbons 1 or 4 to form $C_5H_5CH_3$-1, or to carbons 2 or 3 to form $C_5H_5CH_3$-2. For all of the hydrogen atom additions, the transitional modes consist of 2 angles which can take values to include the front and back side attack of H to R2. Atoms 1 and 4 of R2 are identical to each other so the rate of attack of H atom on carbon 1 is the same as the rate of attack of H atom on carbon 4. Thus the rate coefficient of attack of H atom on carbon 1 is multiplied by 2 to get the total rate coefficient of H addition on R2 to form $C_5H_5CH_3$-1. A similar approach is used to calculate the rate of attack of H atom on R2 to form $C_5H_5CH_3$-2.

Using the approach described above, the rate of formation of $C_5H_5CH_3$-1 from R2 was unexpectedly computed to be slower than the rate of formation of the other two isomers by about 1 order of magnitude. Figure 9 shows the minimum energy pathway for each C−H bond length calculated after randomly selecting 1000 configurations representing different interfragment orientation and calculating the potential at each of those points. It is striking that at a C−H bond distance of 2.9 Å the
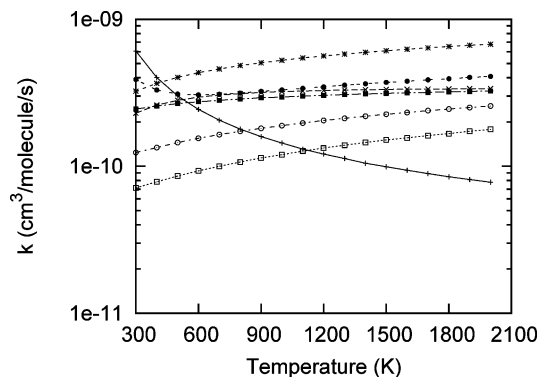
potential is very high for the reaction forming $C_5H_5CH_3$-1. The transition state for formation of $C_5H_5CH_3$-1 at most E and J is located at this interfragment distance. This seems highly suspicious and we have performed an optimization of the R2 + H structure at B3LYP/6-31G(d) level of theory with the distance between carbon atom 1 and H atom frozen at 2.9 Å. This geometry was then used to perform a calculation at CASPT2(6e,6o)/cc-pvtz level of theory to give a barrier height of −15154 cm^{-1} which is very similar to the barrier heights of the other two isomers at 2.9 Å. When we tried to perform a relaxation of the geometry of the transition state for the other two isomers there was no drastic decrease in the barrier. This shows that the high potential value is a consequence of the method we have used, where by we fix the geometry of the fragments at their infinite separation distance. To deal with this problem rigorously one would have to perform the calculation with relaxation of the fragment taken into account. This would increase the complexity of the problem significantly with the angular momentum expressions programmed in Variflex for each of the set of internal coordinates τ in eq 3 changing for each inter fragment separation. This is beyond the scope of the present work. In this work we just remove the point 2.9 Å from our calculations for the $C_5H_5CH_3$-1 isomer which makes the rate of formation of $C_5H_5CH_3$-1 from R2 very similar to the rate of formation of $C_5H_5CH_3$-2, which is what one would expect.

For the addition of c-C_5H_5 to CH_3, the reactants have symmetry numbers of 10 and 6, respectively. The transition state has a symmetry number of 12, which includes a symmetry number of 3 for rotation of CH_3 about the C−C bonding axis, a symmetry number of 2 for the two-dimensional rotational motions of CH_3 about axes perpendicular to the C−C bonding axis, and a symmetry number of 2 for rotation of c-C_5H_5 about axes along the C−H bond on the bonding carbon for c-C_5H_5. Thus the overall path degeneracy is 60/12 = 5 for the five equivalent carbon atoms (equivalent due to the fast pseudorotation) in c-C_5H_5.

The rate coefficients of the barrierless reactions are shown in Figure 10. Also the rate coefficients are fit to a modified Arrhenius form and are provided in Table 7.

3.3. Master Chemical Equation. While using the master equation to calculate the rate coefficients, there are two scenarios in which there are difficulties in calculating the phenomenological rate coefficients from the chemically significant eigenvalues:

1. At low temperatures, the lowest eigenvalue has a very small absolute value. Due to the large difference between the lowest

c-C$_5$H$_5$ + CH$_3$ → Products

J. Phys. Chem. A, Vol. 113, No. 31, 2009 **8879**

TABLE 7: Computed High-Pressure-Limit Rate Coefficients Given in the Form $k = A(T/1000)^n \exp(-E_a/RT)^a$

reactant	product	A	n	E_a
			k_∞	
C$_5$H$_5$CH$_3$-5	C$_5$H$_5$CH$_3$-1	2.8×10^{12}	1.2	24.8
C$_5$H$_5$CH$_3$-1	C$_5$H$_5$CH$_3$-2	3.3×10^{13}	2.1	25.1
c-C$_5$H$_5$ + CH$_3$	C$_5$H$_5$CH$_3$-5	1.1×10^{-10}	−0.7	−0.5
fulvene + H$_2$	C$_5$H$_5$CH$_3$-5	1.2×10^{-7}	3.9	81.1
fulvene + H$_2$	C$_5$H$_5$CH$_3$-1	1.6×10^{-12}	1.4	71.0
fulvene + H$_2$	C$_5$H$_5$CH$_3$-2	1.7×10^{-13}	1.6	55.5
R2 + H	C$_5$H$_5$CH$_3$-5	3.8×10^{-10}	−0.1	0.4
R2 + H	C$_5$H$_5$CH$_3$-1	5.4×10^{-10}	0.3	0.1
R1 + H	C$_5$H$_5$CH$_3$-1	1.1×10^{-10}	0.6	−0.2
R2 + H	C$_5$H$_5$CH$_3$-2	3.0×10^{-10}	0.1	0.0
R3 + H	C$_5$H$_5$CH$_3$-2	1.8×10^{-10}	0.5	−0.1
R4 + H	C$_5$H$_5$CH$_3$-5	2.2×10^{-10}	0.6	−0.8

a The unimolecular rate coefficients are in s^{-1}, and the bimolecular rate coefficients are in cm^3/molecule/s. The units of E_a are kcal/mol.
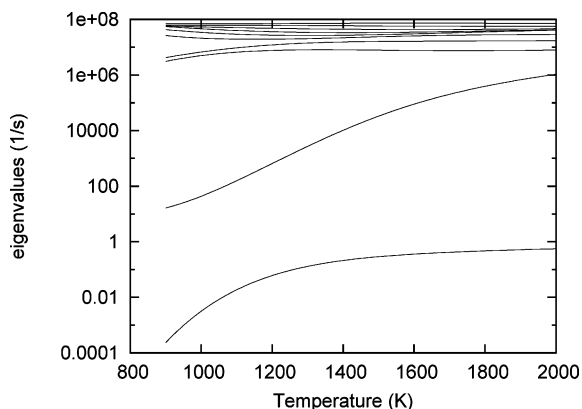

Figure 11. Values of first 10 slowest eigenvalues calculated at various temperatures at 1 atm pressure. Above 1300 K, the fastest two chemically significant eigenvalues become indistinguishable from the rest of the eigenvalues.

magnitude eigenvalue and higher magnitude eigenvalues, computers using 32-bit double precision numbers are not able to calculate the eigenvalue correctly and a spurious positive eigenvalue is obtained.

2. At higher temperatures, some of the chemically significant eigenvalues can merge with eigenvalues associated with collisional relaxation. This condition usually signifies that two species are rapidly equilibrated and essentially act as one chemical species. In other words the rate of conversion between the two species is equal to or faster than the rate of relaxation of internal modes in the two species.

We have plotted the first 10 eigenvalues as a function of temperature at 1 atm pressure in Figure 11. It shows that at almost all temperatures we see that two chemically significant eigenvalues are very close to eigenvalues describing relaxation of internal mode. These two fastest chemically significant eigenvalues correspond to the equilibria between the isomers of the C$_6$H$_8$ adduct. The slowest chemically significant eigenvalue corresponds to the formation of the products from the wells and the reactants and the remaining slow eigenvalue corresponds to the equilibrium between the bimolecular reactants and well species. In the present system, we treat the three rapidly equilibrated well species C$_5$H$_5$CH$_3$-5, C$_5$H$_5$CH$_3$-2, and C$_5$H$_5$CH$_3$-3 as a single species C$_5$H$_5$CH$_3$. To calculate the density of states and partition function of this pseudo species, one would ideally pick out a vibrational mode that is closest to

the intramolecular hydrogen transfer which results in the isomerization of the three isomers. The density of states of this vibrational mode will be replaced by states calculated by solving the Schroedinger equation numerically for the potential energy surface formed by the intramolecular migration of hydrogen atom. This procedure is analogous to the one usually employed to correct for the internal hindered rotors. But in this paper, we have forgone the full procedure in interest of simplicity. We here take one of the isomers and multiply its density of states and partition function by 3 to get the density of states and partition functions of the pseudo species. Because the three isomeric species have very similar ground state energies and vibrational and rotational states the sum of the density of states of the three isomers is very well approximated by multiplying one of the species' density of states by 3. We have confirmed this by carrying out calculations by taking each of these isomers separately and using each of their density of states to calculate the density of state of the pseudo species and the final results for rate coefficients change very little.

With our pseudo species, we reformulate the master chemical equation and obtain 2 chemically significant eigenvalues which are separated from the continuum of eigenvalues. These two eigenvalues can be used to calculate the rate coefficients of interest.

Below 900 K the slowest eigenvalue has a very small magnitude and our eigenvalue solver tends to give a spurious positive value. In this work we have focused primarily on temperatures above 900 K where we can extract accurate rate coefficients.

3.4. Rate Coefficients for c-C$_5$H$_5$ + CH$_3$ → C$_5$H$_5$CH$_3$ and Products. We have calculated the rate of formation of the equilibrated C$_5$H$_5$CH$_3$ and bimolecular products from c-C$_5$H$_5$ + CH$_3$ and have plotted the rate coefficient in Figure 12 for pressure of 1 and 0.01 atm N$_2$. The figures show a more pronounced fall off at lower pressure along with a higher rate of direct conversion of reactant to the products.

Note on Detailed Balance. There are two approximations that are commonly made to calculate the rotational partition function of an asymmetric top because calculating its exact quantum states is computationally demanding. The first one involves treating the three rotations independently and then multiplying the classical partition function of each of them to calculate the total rotational partition function as shown below.

$$Q_{rot} = \frac{\pi^{1/2}}{\sigma} \left(\frac{8\pi^2 I_A k_B T}{h^2} \frac{8\pi^2 I_B k_B T}{h^2} \frac{8\pi^2 I_C k_B T}{h^2} \right)^{1/2}$$

In the second approximation the molecule is treated as a symmetric top even if it is an asymmetric top by calculating the moment of inertia about the degenerate axes I_A as the geometric mean of the moment of inertia about the nearly degenerate axes. With this assumption the rotational partition function Q_{rot} can be calculated as

$$Q_{rot} = \sum_{J=0}^{J_{max}} \sum_{K=-J}^{K=J} (2J + 1) \exp\left(-\frac{J(J + 1)A + (B - A)K^2}{k_B T} \right)$$

where A and B are the rotational constants of the molecule about the degenerate and unique axis respectively and J_{max} is a sufficiently large value. As mentioned in section 2.2.1 to calculate $N(E,J)$ of a molecule Variflex treats it as a symmetric
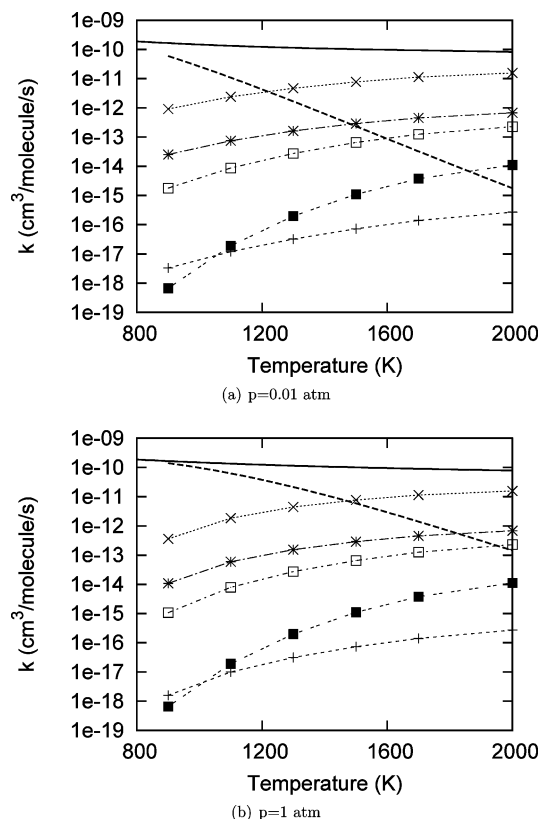
(a) p=0.01 atm

(b) p=1 atm

Figure 12. Rate coefficient of formation of the $C_5H_5CH_3$ species and various bimolecular products from c-C_5H_5 + CH_3 at pressures of 0.01 and 1 atm N_2. The solid line represents high-pressure-limit rate coefficient for recombination of c-C_5H_5 + CH_3, the dashed line represents the actual rate coefficient for reaction c-C_5H_5 + CH_3 → $C_5H_5CH_3$. The rest of the lines represent rate coefficients to products where, + corresponds to fulvene + H_2; × corresponds to R2 + H; * corresponds to R1 + H; □ corresponds to R3 + H; ■ corresponds to R4 + H_2.

Figure 13. The "+" signs are measurements of $C_5H_5CH_3$-5 decomposition by Ikeda et al.[40] at 100−400 Torr Kr and the solid line is from calculations performed at 200 Torr Kr using $\langle \Delta E_d \rangle$ = 350 cm^{-1}. The solid boxes are measurements by Lifshitz et al.[50] at 2.71 atm Ar; the dotted line is from calculations at the same pressure using $\langle \Delta E_d \rangle$ = 150 × (T/300) cm^{-1} and the dashed line is using $\langle \Delta E_d \rangle$ = 100 cm^{-1}.
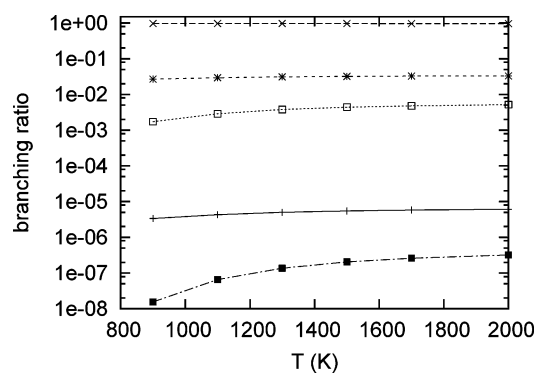
Figure 14. Branching ratio for each product channel from decomposition of $C_5H_5CH_3$ at 1 atm N_2. + corresponds to fulvene + H_2; × corresponds to R2 + H; * corresponds to R1 + H; □ corresponds to R3 + H; ■ corresponds to R4 + H_2.

top. The partition function calculated by the two approximations can differ from each other by about 10%. Thus if the partition function is calculated using the first approximation and as mentioned in section 2.2.1 the second approximation is used to calculate the density of states used in the master equation the detailed balance is not satisfied. This shows the importance of calculating the partition function and density of states in a consistent manner.

In Figure 13 we plot the rate coefficient for the decomposition of 5-methylcyclopentadiene in Kr measured in a shock tube by Ikeda et al.[40] against the rate coefficient predicted by our calculations for a pressure of 200 Torr. Also on the same graph is plotted the decomposition rate of methylcyclopentadiene in Ar measured in a shock tube at pressures of 2.71 atm by Lifshitz et al.[50] The calculated rate coefficients at 200 Torr Kr are systematically higher than the rate coefficients measured by Ikeda et at. by about a factor of 2 for all of the temperatures measured. This factor of 2 is well within the error bounds of the calculations. For the comparison with data by Lifshitz we have performed calculations using two different energy transfer parameters for Ar gas. When we use the value of $\langle \Delta E_d \rangle$ = 150 × (T/300) cm^{-1}, which has been recommended by Golden et al.[51] we get about a fact of 5 difference between calculated results and experimental measurements, but when we change this value to $\langle \Delta E_d \rangle$ = 100 cm^{-1} the agreement becomes much better. $\langle \Delta E_d \rangle$ values have large uncertainties and it is difficult to pin down an exact value a priori. In this study we have chosen
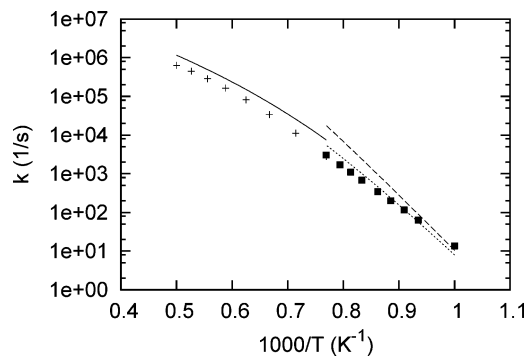
to use the value of $\langle \Delta E_d \rangle$ = 100 for Ar to carry out the rest of the calculations because this value gives good agreement with the experimental results. We should note that the error in the calculated values of the rate coefficients can be as high at a factor of 5 as is shown in section 3.5.

3.5. Rate Coefficients of Formation of Bimolecular Products from $C_5H_5CH_3$. The rate of formation of bimolecular products is one of the most important results of this study. The C_6H_7 products further lose a hydrogen atom and then isomerize to form benzene. In the literature many pathways have been mentioned which lead to benzene formation from C_6H_7.[2,52] In some practical situations these C_6H_7 molecules are formed predominantly by the pathways in Figure 1. At most temperatures and pressures the formation of R2 is about an order of magnitude greater than the second fastest forming product R1 + H (see Figure 14). However R2 does not have a direct route that leads to the formation of benzene without going through one of the other C_6H_7 radicals. To calculate the formation of benzene from these C_6H_7 radicals, a similar analysis as the one presented in this paper needs to be performed.

The rate coefficients for all of the pressure dependent reactions at various pressures and temperatures in N_2 bath gas are given in Tables 8 and 9. Rate coefficients for all these reactions in Ar bath gas are included in the Supporting Information.

Uncertainties in Calculated Rates. The rates calculated in Tables 8 and 9 are based on a long series of calculation steps

TABLE 8: Rate Coefficients for Various Reactions in the Temperature Range 900−2000 K at 0.01 and 1 atm Pressure N$_2$[a]

reactions	temperatures (K)					
	900	1100	1300	1500	1700	2000
p = 0.01 atm						
c-C$_5$H$_5$ + CH$_3$ → C$_5$H$_5$CH$_3$	5.9×10^{-11}	1.2×10^{-11}	1.8×10^{-12}	2.3×10^{-13}	3.1×10^{-14}	1.8×10^{-15}
c-C$_5$H$_5$ + CH$_3$ → fulvene + H$_2$	3.3×10^{-18}	1.2×10^{-17}	3.2×10^{-17}	7.3×10^{-17}	1.4×10^{-16}	2.7×10^{-16}
c-C$_5$H$_5$ + CH$_3$ → R2 + H	9.1×10^{-13}	2.4×10^{-12}	4.7×10^{-12}	7.8×10^{-12}	1.1×10^{-11}	1.6×10^{-11}
c-C$_5$H$_5$ + CH$_3$ → R1 + H	2.5×10^{-14}	7.5×10^{-14}	1.6×10^{-13}	2.9×10^{-13}	4.6×10^{-13}	6.8×10^{-13}
c-C$_5$H$_5$ + CH$_3$ → R3 + H	1.8×10^{-15}	8.8×10^{-15}	2.8×10^{-14}	6.5×10^{-14}	1.3×10^{-13}	2.3×10^{-13}
c-C$_5$H$_5$ + CH$_3$ → R4 + H	6.8×10^{-19}	1.9×10^{-17}	2.0×10^{-16}	1.1×10^{-15}	3.8×10^{-15}	1.1×10^{-14}
C$_5$H$_5$CH$_3$ → c-C$_5$H$_5$ + CH$_3$	9.3×10^{-2}	2.3×10^{1}	4.4×10^{2}	2.4×10^{3}	7.0×10^{3}	2.2×10^{4}
C$_5$H$_5$CH$_3$ → fulvene + H$_2$	2.3×10^{-10}	7.7×10^{-8}	1.7×10^{-6}	9.3×10^{-6}	2.8×10^{-5}	8.5×10^{-5}
C$_5$H$_5$CH$_3$ → R2 + H	1.1×10^{-4}	3.6×10^{-2}	8.0×10^{-1}	4.6×10^{0}	1.4×10^{1}	4.5×10^{1}
C$_5$H$_5$CH$_3$ → R1 + H	2.5×10^{-6}	8.1×10^{-4}	1.8×10^{-2}	1.0×10^{-1}	3.2×10^{-1}	1.0×10^{0}
C$_5$H$_5$CH$_3$ → R3 + H	3.5×10^{-8}	1.2×10^{-5}	2.4×10^{-4}	1.1×10^{-3}	2.4×10^{-3}	5.5×10^{-3}
C$_5$H$_5$CH$_3$ → R4 + H	*b*	*b*	*b*	*b*	*b*	*b*
p = 1 atm						
c-C$_5$H$_5$ + CH$_3$ → C$_5$H$_5$CH$_3$	1.4×10^{-10}	7.3×10^{-11}	2.5×10^{-11}	6.5×10^{-12}	1.4×10^{-12}	1.4×10^{-13}
c-C$_5$H$_5$ + CH$_3$ → fulvene + H$_2$	1.6×10^{-18}	1.0×10^{-17}	3.1×10^{-17}	7.2×10^{-17}	1.4×10^{-16}	2.7×10^{-16}
c-C$_5$H$_5$ + CH$_3$ → R2 + H	3.6×10^{-13}	1.8×10^{-12}	4.4×10^{-12}	7.7×10^{-12}	1.1×10^{-11}	1.6×10^{-11}
c-C$_5$H$_5$ + CH$_3$ → R1 + H	1.1×10^{-14}	5.9×10^{-14}	1.5×10^{-13}	2.9×10^{-13}	4.5×10^{-13}	6.8×10^{-13}
c-C$_5$H$_5$ + CH$_3$ → R3 + H	1.1×10^{-15}	7.8×10^{-15}	2.7×10^{-14}	6.5×10^{-14}	1.3×10^{-13}	2.3×10^{-13}
c-C$_5$H$_5$ + CH$_3$ → R4 + H	6.6×10^{-19}	1.9×10^{-17}	2.0×10^{-16}	1.1×10^{-15}	3.8×10^{-15}	1.1×10^{-14}
C$_5$H$_5$CH$_3$ → c-C$_5$H$_5$ + CH$_3$	2.2×10^{-1}	1.4×10^{2}	6.1×10^{3}	5.5×10^{4}	2.2×10^{5}	8.3×10^{5}
C$_5$H$_5$CH$_3$ → fulvene + H$_2$	3.0×10^{-9}	3.9×10^{-6}	2.5×10^{-4}	2.7×10^{-3}	1.2×10^{-2}	5.0×10^{-2}
C$_5$H$_5$CH$_3$ → R2 + H	9.9×10^{-4}	1.1×10^{0}	6.9×10^{1}	7.3×10^{2}	3.1×10^{3}	1.3×10^{4}
C$_5$H$_5$CH$_3$ → R1 + H	2.6×10^{-5}	3.1×10^{-2}	1.9×10^{0}	2.1×10^{1}	9.0×10^{1}	3.8×10^{2}
C$_5$H$_5$CH$_3$ → R3 + H	1.2×10^{-6}	1.9×10^{-3}	1.3×10^{-1}	1.5×10^{0}	6.7×10^{0}	2.9×10^{1}
C$_5$H$_5$CH$_3$ → R4 + H	3.2×10^{-11}	9.2×10^{-8}	8.4×10^{-6}	1.1×10^{-4}	5.1×10^{-4}	2.2×10^{-3}

[a] In this table, C$_5$H$_5$CH$_3$ represents equilibrated isomers. The unimolecular rate coefficients are in s^{-1}, and the bimolecular rate coefficients are in cm^3/molecule/s. [b] Too slow to be computed accurately using eigenvalue approach at double precision.

TABLE 9: Rate Coefficients for Various Reactions in the Temperature Range 900−2000 K at 10 and 100 atm Pressure N$_2$[a]

reactions	temperatures (K)					
	900	1100	1300	1500	1700	2000
p = 10 atm						
C$_5$H$_5$ + CH$_3$ → C$_5$H$_5$CH$_3$	1.5×10^{-10}	1.1×10^{-10}	5.8×10^{-11}	2.3×10^{-11}	7.1×10^{-12}	1.0×10^{-12}
c-C$_5$H$_5$ + CH$_3$ → fulvene +H$_2$	5.0×10^{-19}	6.1×10^{-18}	2.7×10^{-17}	7.0×10^{-17}	1.4×10^{-16}	2.7×10^{-16}
c-C$_5$H$_5$ + CH$_3$ → R2 + H	9.9×10^{-14}	9.8×10^{-13}	3.5×10^{-12}	7.2×10^{-12}	1.1×10^{-11}	1.6×10^{-11}
c-C$_5$H$_5$ + CH$_3$ → R1 + H	3.1×10^{-15}	3.3×10^{-14}	1.3×10^{-13}	2.7×10^{-13}	4.5×10^{-13}	6.8×10^{-13}
c-C$_5$H$_5$ + CH$_3$ → R3 + H	3.8×10^{-16}	5.1×10^{-15}	2.4×10^{-14}	6.4×10^{-14}	1.2×10^{-13}	2.3×10^{-13}
c-C$_5$H$_5$ + CH$_3$ → R4 + H	4.8×10^{-19}	1.8×10^{-17}	2.0×10^{-16}	1.1×10^{-15}	3.8×10^{-15}	1.1×10^{-14}
C$_5$H$_5$CH$_3$ → c-C$_5$H$_5$ + CH$_3$	2.4×10^{-1}	2.0×10^{2}	1.4×10^{4}	1.8×10^{5}	9.2×10^{5}	4.2×10^{6}
C$_5$H$_5$CH$_3$ → fulvene +H$_2$	4.7×10^{-9}	1.2×10^{-5}	1.4×10^{-3}	2.5×10^{-2}	1.5×10^{-1}	7.7×10^{-1}
C$_5$H$_5$CH$_3$ → R2 + H	1.4×10^{-3}	2.8×10^{0}	3.0×10^{2}	5.1×10^{3}	2.9×10^{4}	1.5×10^{5}
C$_5$H$_5$CH$_3$ → R1 + H	3.8×10^{-5}	8.2×10^{-2}	9.2×10^{0}	1.6×10^{2}	9.1×10^{2}	4.7×10^{3}
C$_5$H$_5$CH$_3$ → R3 + H	2.3×10^{-6}	7.2×10^{-3}	9.5×10^{-1}	1.8×10^{1}	1.1×10^{2}	5.9×10^{2}
C$_5$H$_5$CH$_3$ → R4 + H	3.4×10^{-10}	2.7×10^{-6}	5.5×10^{-4}	1.3×10^{-2}	9.1×10^{-2}	5.5×10^{-1}
p = 100 atm						
c-C$_5$H$_5$ + CH$_3$ → C$_5$H$_5$CH$_3$	1.6×10^{-10}	1.2×10^{-10}	9.1×10^{-11}	5.4×10^{-11}	2.5×10^{-11}	5.8×10^{-12}
c-C$_5$H$_5$ + CH$_3$ → fulvene + H$_2$	8.6×10^{-20}	2.1×10^{-18}	1.6×10^{-17}	5.8×10^{-17}	1.3×10^{-16}	2.7×10^{-16}
c-C$_5$H$_5$ + CH$_3$ → R2 + H	1.5×10^{-14}	2.8×10^{-13}	1.8×10^{-12}	5.4×10^{-12}	1.0×10^{-11}	1.5×10^{-11}
c-C$_5$H$_5$ + CH$_3$ → R1 + H	5.0×10^{-16}	1.0×10^{-14}	6.7×10^{-14}	2.1×10^{-13}	4.1×10^{-13}	6.7×10^{-13}
c-C$_5$H$_5$ + CH$_3$ → R3 + H	6.9×10^{-17}	1.8×10^{-15}	1.5×10^{-14}	5.3×10^{-14}	1.2×10^{-13}	2.2×10^{-13}
c-C$_5$H$_5$ + CH$_3$ → R4 + H	1.6×10^{-19}	1.1×10^{-17}	1.7×10^{-16}	1.1×10^{-15}	3.7×10^{-15}	1.1×10^{-14}
C$_5$H$_5$CH$_3$ → c-C$_5$H$_5$ + CH$_3$	2.5×10^{-1}	2.3×10^{2}	2.2×10^{4}	4.3×10^{5}	2.9×10^{6}	1.7×10^{7}
C$_5$H$_5$CH$_3$ → fulvene + H$_2$	5.4×10^{-9}	2.0×10^{-5}	4.2×10^{-3}	1.3×10^{-1}	1.2×10^{0}	8.8×10^{0}
C$_5$H$_5$CH$_3$ → R2 + H	1.5×10^{-3}	4.2×10^{0}	7.4×10^{2}	2.1×10^{4}	1.7×10^{5}	1.2×10^{6}
C$_5$H$_5$CH$_3$ → R1 + H	4.2×10^{-5}	1.3×10^{-1}	2.4×10^{1}	7.1×10^{2}	6.1×10^{3}	4.3×10^{4}
C$_5$H$_5$CH$_3$ → R3 + H	2.8×10^{-6}	1.4×10^{-2}	3.4×10^{0}	1.1×10^{2}	1.0×10^{3}	7.8×10^{3}
C$_5$H$_5$CH$_3$ → R4 + H	8.8×10^{-10}	1.7×10^{-5}	8.0×10^{-3}	3.8×10^{-1}	4.3×10^{0}	3.9×10^{1}

[a] In this table, C$_5$H$_5$CH$_3$ represents equilibrated isomers. The unimolecular rate coefficients are in s^{-1}, and the bimolecular rate coefficients are in cm^3/molecule/s.

each of which have uncertainties and approximations associated with them. The cumulative effect of all these uncertainties are difficult to quantify, but we feel that it is useful to have an estimate on the uncertainties of the rate coefficients.

For most of the calculations performed we have used the CBS-QB3 compound method to calculate the energies of molecules and saddle points. This method is expected to typically have an error of about 2 kcal/mol. Based on this

we assume that the error in the barrier heights can be about 2 kcal/mol. The density of states and frequencies are usually calculated more accurately than the energy, so we expect the error in entropies to be less than 1.5 cal/mol/K. A 2 kcal/mol error in enthalpy and 1.5 cal/mol/K error in entropy translates to an uncertainty in the computed rate coefficients of about a factor of 5 at 1000 K.

4. Conclusion

In this paper, we have calculated the high-pressure-limit and pressure dependent rate coefficients for all of the reactions in Figure 1. We have compared our calculations against shock tube experiments and the comparison is quite good. We see a significant amount of fall off and chemical activation in the pressure dependent network and using high pressure rate coefficients for these reactions would not be appropriate. The rate coefficients computed here will be helpful in understanding the formation of aromatic rings in combustion.

Supporting Information Available: Python code to calculate the energy levels and entropy for Jahn−Teller active mode is included. Cartesian coordinates, harmonic vibrational frequencies and principal moments of inertia of all the molecules and transition states are given. Also rate coefficients of all the reactions at 0.01, 1, 10, and 100 atm Ar are given. This material is available free of charge via the Internet at http://pubs.acs.org.

References and Notes

(1) McEnally, C. S.; Pfefferle, L. D. *Combust. Sci. Technol.* **1998**, *131*, 323–344.

(2) Melius, C. F.; Colvin, M. E.; Marinov, N. M.; Pitz, W. J.; Senkan, S. M. *Proc. Combust. Inst.* **1996**, *26*, 685–692.

(3) Moskaleva, L. V.; Mebel, A. M.; Lin, M. C. *Proc. Combust. Inst.* **1996**, *26*, 521–526.

(4) Harding, L.; Georgievskii, Y.; Klippenstein, S. *J. Phys. Chem. A* **2005**, *109*, 4646–4656.

(5) Jasper, A. W.; Klippenstein, S. J.; Harding, L. B.; Ruscic, B. *J. Phys. Chem. A* **2007**, *111*, 3932–3950.

(6) Harding, L. B.; Klippenstein, S. J.; Georgievskii, Y. *Proc. Combust. Inst.* **2005**, *30*, 985–993.

(7) Klippenstein, S. J.; Georgievskii, Y.; Harding, L. B. *Phys. Chem. Chem. Phys.* **2006**, *8*, 1133–1147.

(8) Klippenstein, S. J.; Miller, J. A. *J. Phys. Chem. A* **2002**, *106*, 9267–9277.

(9) Miller, J. A.; Klippenstein, S. J. *J. Phys. Chem. A* **2000**, *104*, 2061–2069.

(10) Miller, J. A.; Klippenstein, S. J. *J. Phys. Chem. A* **2001**, *105*, 7254–7266.

(11) Miller, J. A.; Klippenstein, S. J. *J. Phys. Chem. A* **2003**, *107*, 2680–2692.

(12) Miller, J. A.; Klippenstein, S. J.; Raffy, C. *J. Phys. Chem. A* **2002**, *106*, 4904–4913.

(13) Miller, J. A.; Klippenstein, S. J.; Robertson, S. H. *J. Phys. Chem. A* **2000**, *104*, 7525–7536.

(14) Frisch, M. J.; et al. *Gaussian 03, Revision C.02*, Gaussian, Inc., Wallingford, CT, 2004.

(15) Montgomery, J. A.; Ochterski, J. W.; Petersson, G. A. *J. Chem. Phys.* **1994**, *101*, 5900–5909.

(16) Ochterski, J. W.; Petersson, G. A.; Montgomery, J. A. *J. Chem. Phys.* **1996**, *104*, 2598–2619.

(17) Montgomery, J. A.; Frisch, M. J.; Ochterski, J. W.; Petersson, G. A. *J. Chem. Phys.* **2000**, *112*, 6532–6542.

(18) Curtiss, L. A.; Raghavachari, K.; Trucks, G. W.; Pople, J. A. *J. Chem. Phys.* **1991**, *94*, 7221–7230.

(19) Curtiss, L. A.; Raghavachari, K.; Redfern, P. C.; Pople, J. A. *J. Chem. Phys.* **1997**, *106*, 1063–1079.

(20) Celani, P.; Werner, H.-J. *J. Chem. Phys.* **2000**, *112*, 5546–5557.

(21) Werner, H.-J. *Mol. Phys.* **1996**, *89*, 645–661.

(22) Werner, H.-J.; et al. MOLPRO, version 2006. 1, a package of ab initio programs, 2006.

(23) Scott, A. P.; Radom, L. *J. Phys. Chem.* **1996**, *100*, 16502–16513.

(24) Pitzer, K. S.; Gwinn, W. D. *J. Chem. Phys.* **1942**, *10*, 428–440.

(25) Pitzer, K. S. *J. Chem. Phys.* **1946**, *14*, 239–243.

(26) Kilpatrick, J. E.; Pitzer, K. S. *J. Chem. Phys.* **1949**, *17*, 1064–1075.

(27) East, A. L. L.; Radom, L. *J. Chem. Phys.* **1997**, *106*, 6655–6674.

(28) Petersson, G. A.; Malick, D. K.; Wilson, W. G.; Ochterski, J. W.; Montgomery, J. A.; Frisch, M. J. *J. Chem. Phys.* **1998**, *109*, 10570–10579.

(29) Hirschfelder, J. O.; Wigner, E. *J. Chem. Phys.* **1939**, *7*, 616–628.

(30) Miller, J. A.; Parrish, C.; Brown, N. J. *J. Phys. Chem.* **1986**, *90*, 3339–3345.

(31) Marcus, R. A. *J. Chem. Phys.* **1952**, *20*, 359–364.

(32) Marcus, R. A.; Rice, O. K. *J. Phys. Colloid Chem.* **1951**, *55*, 894–908.

(33) Wardlaw, D. M.; Marcus, R. A. *Chem. Phys. Lett.* **1984**, *110*, 230–234.

(34) Wardlaw, D. M.; Marcus, R. A. *J. Chem. Phys.* **1985**, *83*, 3462–3480.

(35) Wardlaw, D. M.; Marcus, R. A. *J. Phys. Chem.* **1986**, *90*, 5383–5393.

(36) Klippenstein, S. *J. Phys. Chem.* **1994**, *98*, 11459–11464.

(37) Malick, D. K.; Petersson, G. A.; Montgomery, J. A. *J. Chem. Phys.* **1998**, *108*, 5704–5713.

(38) Fernandez-Ramos, A.; Miller, J.; Klippenstein, S.; Truhlar, D. *Chem. Rev.* **2006**, *106*, 4518–4584.

(39) Miller, J.; Klippenstein, S. *J. Phys. Chem. A* **2006**, *110*, 10528–10544.

(40) Ikeda, E.; Tranter, R. S.; Kiefer, J. H.; Kern, R. D.; Singh, H. J.; Zhang, Q. *Proc. Combust. Inst.* **2000**, *28*, 1725–1732.

(41) Curtiss, L. A.; Raghavachari, K.; Redfern, P. C.; Rassolov, V.; Pople, J. A. *J. Chem. Phys.* **1998**, *109*, 7764–7776.

(42) Barckholtz, T. A.; Miller, T. A. *Int. Rev. Phys. Chem.* **1998**, *17*, 435–524.

(43) Kiefer, J. H.; Tranter, R. S.; Wang, H.; Wagner, A. F. *Int. J. Chem. Kinet.* **2001**, *33*, 834–845.

(44) Katzer, G.; Sax, A. F. *J. Chem. Phys.* **2002**, *117*, 8219–8228.

(45) Longuet-Higgins, H. C. *Advances in Spectroscopy Volume II*; Interscience Publishers Inc., New York, 1961.

(46) Fischer, G. *Vibronic Coupling: The Interaction between the Electronic and Nuclear Motions*; Academic Press, 1984.

(47) Applegate, B. E.; Miller, T. A.; Barckholtz, T. A. *J. Chem. Phys.* **2001**, *114*, 4855–4868.

(48) Applegate, B. E.; Bezant, A. J.; Miller, T. A. *J. Chem. Phys.* **2001**, *114*, 4869–4882.

(49) Amos, R. D.; Alberts, I. L.; S., A. J. *Cambridge Analytical Derivative Package (CADPAC), Issue 5.2*, University of Cambridge, Cambridge, UK, 1995.

(50) Lifshitz, A.; Tamburu, C.; Suslensky, A.; Dubnikova, F. *Proc. Combust. Inst.* **2005**, *30*, 1039–1047.

(51) Golden, D. M. *Chem. Soc. Rev.* **2008**, *37*, 717–731.

(52) Dubnikova, F.; Lifshitz, A. *J. Phys. Chem. A* **2002**, *106*, 8173–8183.